The role of peri-glacial Active Layer Development in determining soil-regolith thickness across a Triassic sandstone outcrop in the UK.

*A.M. Tye, S.J. Kemp, Lark, R.M. & A.E. Milodowski
British Geological Survey, Kingsley Dunham Centre, Keyworth, Nottingham, NG12 5GG.

*Author for correspondence
e-mail: atye@bgs.ac.uk
Tel: 0115 9363229
Fax: 0115 9363264

Keywords: Sherwood Sandstone, Regolith, Weathering, Soil Thickness, Active Layer development

Abstract

This paper examines the weathering processes that have combined to produce the distribution of soil-regolith (SR) thickness across the Triassic Sherwood Sandstone Group outcrop (750 km^2) in Nottinghamshire, U.K. Archive borehole logs (n=282) taken across the outcrop showed that soil-regolith thickness had mean and median depths of ~1.8 and 1.5m respectively. Cores were taken from a forested site to depths ~3m for geochemical analysis. At this site the SR thickness was ~1.7m. Analysis of the loss of elements, compared to bedrock using mass balance calculations (τ) showed that all the calcite and gypsum cement had been removed to depths of >3m. Thus the major difference between the SR and the underlying saprolite was that the former exists as loose sand as opposed to a semi-durable rock. Scanning electron microscopy (SEM) analysis of core samples suggested that the non-durable rock or saprolite had greater cementation of clay particles. We propose that the mechanism through which the clay cement (and other interlocking grain bonds) were eased apart was through freeze-thaw processes associated with the summer 'active layer development' during the last glacial activity in the UK. We tested this theory by developing a Monte Carlo simulation based on a simplified version of the Stefan Equation. Current Arctic datasets of air and ground temperatures were obtained to provide reasonable starting conditions for input variables. These were combined with known data for thermal conductivity, bulk density and moisture content of the Sherwood Sandstone regolith. Model predictions (n=1000) of the distribution of SR thickness accurately reflect the observed distribution thickness from the borehole logs. This is strong evidence that freeze-thaw and 'ALD' processes are major factors in determining the thickness of SR across this outcrop.

Introduction

Soil and regolith thickness is important as it contributes to functions such as carbon, nutrient and water storage as well as filtering capacity. Knowledge of how soil-regolith (SR) thickness varies over relatively large areas and parent materials is limited. Two such studies are those undertaken by Phillips *et al*. (2005) and Hren *et al*. (2007). The former examined SR thickness in the Ouachita Mountains on Paleozoic sedimentary rocks whilst the latter surveyed 225 locations in the Washington Cascades. A third study by Tye *et al*. (2011), examined the distribution of (i) weathering depths to bedrock and (ii) soil-regolith (SR) thickness across a Triassic sandstone outcrop (750 km^2) in the East Midlands of the UK. Their results reported a median SR depth of 1.6m, whilst weathering depth from surface to bedrock (including saprolite or non-durable rock) was generally between 4-6m.

In this paper we examine the weathering processes responsible for generating the mobile SR across the Sherwood Sandstone outcrop as previously reported (Tye *et al*., 2011) that constitutes the uppermost part of the weathering continuum (Spink & Norberry, 1993). Since early investigations by Davies (1892) and Gilbert (1909), the concept of convex hillslopes and 'steady-state' conditions has been central to many studies of soil thickness. Despite the concept of 'steady-state' being implicit in many landscape evolution models, there are few examples where steady-state soil thickness is observable (Phillips, 2010). In addition, an early hypothesis proposed by Gilbert (1909) suggested that the rate of SR production or bedrock lowering is determined by the thickness of the SR itself, contributing to a negative feedback relationship, with both the distribution of moisture and heat playing critical roles in determining the rate of the weathering process. This has been described as the 'soil production function' and its shape can be either humped or linear (Heimsath, 1997). Recent advancements using cosmogenic radionuclides such as ^{10}Be and ^{26}Al have explored the 'soil production function' more fully (e.g.

Heimsath *et al.* 2001; Small *et al*. 1999; Burke *et al*. 2007; amongst others). The depths at which maximum SR production or bedrock lowering can occur have been found to be bedrock and/or climate dependent. For example, maximum SR production rates have been determined as 50m / Myr for fractured granite in SW Australia (Heimsath *et al*. 2000), 2080m / Myr for marine shales (McKean *et al*. 1993) and 10m / Myr for sandstone in Australia. (Heimsath *et al*. 2009). In the U.K. few data are available relating to the use of cosmogenic radionuclides to measure bedrock lowering. However, Riggins *et al*. (2011) found SR production rates on the granite rocks of Bodmin Moor, England, to be 10-20m / Myr. Maximum SR production rates determined using cosmogenic radionuclide analyses have been found to occur under soil depths of between 15 and 100cm (Small *et al*. 1999; Burke *et al*. 2007; Riggins *et al*. 2011). For soils formed from sandstones, Heimsath *et al*. 2009 found that maximum SR production rates occurred at depths of ~35cm in Arnhem Land, Australia.

Beyond bedrock lowering by chemical and physical weathering processes, there are additional factors contributing to the variation in SR thickness including non-linear transport processes such as shallow landsliding (Roering *et al*., 2001), glacial / periglacial processes such as gelifluction (Carter & Ciolkosz, 1986), tree throw (Carter & Ciolkosz, 1991) and bioturbation by burrowing animals such as pocket gophers (Yoo *et al.* 2005). However, the 'soil production function' and the concept of 'steady-state' have been used to constrain many theoretical and measurement-based soil thickness and bedrock lowering models (e.g. Braun *et al*. 2001; Misasny & McBratney, 1999; Mudd and Furbish 2004; Fernandes & Dietrich, 1997; Yoo *et al*. 2009).

When assessing likely processes contributing to SR thickness on regional scales, the influence of tectonics and how it controls uplift, fracturing and weathering of new rock has been considered (Berner *et al*. 1983; Molnar *et al*. 2007). In the Washington Cascades, Hren *et al*. (2007) identified the weathering zone depth and rock exhumation rate as being important in explaining dissolved Si fluxes. Additionally, increased weathering has been found around regional faulting and associated smaller fractures in rocks as they can act as drainage networks (Milodowski *et al*. 1998; Akhurst *et al*. 1998). Digital Terrain Models (DTM's) have been used to explore relationships between slope properties and soil thickness on regional scales. However, generally only weak relationships have been found. Hren *et al.* (2007) found a weak relationship (R^2 = 0.27) between log slope angle (m/m) and log soil depth in their study. Phillips *et al*. (2005) found that despite individual slopes showing relationships between slope characteristics and soil thickness there were no significant relationships between soil thickness, slope angle and curvature in their wider survey in the Ouachita Mountains. Similarly, Tye *et al*. (2011) found no relationships between landscape characteristics and soil thickness across a sandstone outcrop. A further finding from this study was that there was only a very weak Spearman's Rank correlation (r_s = 0.25, p<0.001, n=192) between the soil depth and total weathered depth to bedrock. This result suggests that the weathering process was not just chemical (e.g. dissolution of carbonate, anhydrite and gypsum cements (Burley & Kantorowicz, 1986; Bath *et al*. 1987) but also required a physical weathering process to develop the mobile SR thickness.

One physical weathering process that could influence the spatial distribution of the SR across the Sherwood Sandstone outcrop, and is likely to have been widespread in the UK is that of Active Layer Development (ALD) and seasonal freeze thaw during the peri-glacial climates that affected the UK around the Last Glacial Maximum (~19000 BP). A review of depths of 'ALD' in current polar regions reveals similar values to the mean and median values of soil thickness found in our original study (Tye *et al*. 2011). For example, in Antarctica, Adlam *et al*. (2010) found that at latitude 77° South, active layers were > 90cm. Leszkiewicz and Caputa (2004) examined ALD at Hornsund, Spitsbergen and found the thawed layer extended to ~1.3 m whilst Wollschalager *et al*. (2010) found the thickness of the active layer in bare soil to extend to ~1.6 m at a permafrost site on the Tibetan plateau. Klene *et al*. (2001) found that the extent of ALD influenced locally by vegetation cover, rock type, porosity, peat or snow cover and soil moisture.

This study builds on the work of a previous paper (Tye *et al*. 2011) which examined the factors influencing the spatial distribution of weathering depths to competent bedrock. In this paper we specifically address the issues related to the distribition of SR depths across the Sherwood Sandstone outcrop. Firstly, we examine the long-term chemical weathering processes in relation to the physical properties of the soil-regolith-saprolite. Secondly, we propose that periglacial activity and 'active layer development' (ALD) has left a physical weathering imprint on the thickness of the soil and regolith by breaking the clay cement that had previously held the soil-regolith intact after the carbonate and gypsum cements had been removed. Thirdly, we test this proposal by applying a Monte Carlo simulation based on the Stefan equation for predicting the depth of 'ALD' (Klene *et al.*, 2001) to describe the likely distribution of soil thickness across the outcrop if this process was a major control on soil thickness.

2. Materials and Methods

2.1 Study area

The study area (outcrop) is situated in the county of Nottinghamshire, U.K., and is approximately 50 km long and 15 km wide (750 km^2). It is a gentle, undulating low relief landscape. A full description of the geology can be found in Tye *et al*. (2011). The Quaternary history of the study area is poorly understood. The area was last glaciated during the Anglian period (450 000 BP) although two subsequent major glaciations have occurred during which the area would have been subjected to intense periglacial weathering. Evidence of periglacial climates have been found in the form of ice-wedge casts in the Holme Pierrepoint sand and gravel terraces of the River Trent (Howard *et al.* 2009) aged ~26000 yrs BP. It is assumed that the Sherwood Sandstone Group outcrop has largely been weathered in-situ leaving a soil, classified by the Soil Survey of England and Wales as the Cuckney Series, described as very slightly stony sand to a depth of ~70 cm, with sand below (Ragg *et al*., 1984). Land-use on about 80 % of the outcrop is agriculture (mainly arable) and ~18 % is either deciduous or coniferous woodland. In Tye *et al*. (2011) a full weathering description of the profile is presented. The profile consists of a top section of soil and loose sand which we refer to as the 'soil-regolith' and which at the base soil production is initiated. Beneath the soil-regolith is the 'saprolite' or non-durable rock (an engineering geology description; Spink & Norberry, 1993) of variable thickness overlying hard or competent sandstone. The spatial variation of the saprolite thickness is reported in Tye *et al*. (2011).

2.2 Collection of samples and archive data

2.2.1 Borehole logs

The National Geoscience Data Centre (NGDC) at the British Geological Survey holds information recorded from the majority of boreholes (>10m in length) taken in the UK. A total of ~2500 borehole records were identified from the study area; of these 282 had information relating to the thickness of the SR which was recorded along with the borehole's grid reference. The borehole records were mostly produced by engineers during road construction and the drilling of water abstraction wells. Figure 1 shows the borehole distribution across the Sherwood Sandstone outcrop, along with the SR depth.

2.2.2 Soil-regolith-saprolite core sampling and Bedrock Sandstone samples

Cores (n=4) of SR and saprolite (diameter 7.5cm) were extracted from a mixed woodland site in Sherwood Forest (British National Grid: 461100m Easting 362300m Northing) to depths of ~3m using a vibracore drilling rig. Once extracted the cores were placed at 4°C in a core store, prior to being cut into 30cm sections. The core material was air dried before being disaggregated to < 2mm for geochemical analysis. One core was cut to calculate the variation of bulk density with depth. Samples of sandstone from different depths (3, 6, 7, 17m) were collected from the Bestwood Quarry in Nottinghamshire (British National Grid: 456800m Easting 352000m Northing), approximately ~10 km from the site that the SR cores were collected. In addition, we analysed samples of Sherwood Sandstone Group Bedrock from a depths of ~50m from Gamston in Lincolnshire (British National Grid: 470330m Easting 376550m Northing), approximately 30 km to the NE (Bath *et al*. 1987). These samples represent a range of Sherwood Sandstone Group lithologies which can be used to compare the nature of weathering processes in soil, near-surface rock and deeper bedrock.

2.3 Physical characterization of samples and regolith

Bulk density of the fine earth (< 2 mm) fraction was determined by the method of Smith & Thomasson (1982) on each of the 30cm sections, taking into account the weight and volume of stones (>2mm). Particle density was calculated using a pycnometer according to BS 1377: Part 2 (1990) and results were used in the determination of % porosity by volume of each segment of the core using equation 1.

$$\%Porosity = \left(1 - \frac{BulkDensity}{ParticleDensity}\right)100 \qquad \text{eqn. 1}$$

Changes in the resistance of the SR at the Sherwood Forest site was measured in the field using a Panda penetrometer (Langton, 1999). Measurements were made to depths of ~2.5m.

2.4 Geochemical analysis

Total soil element concentrations were determined by X-ray fluorescence spectroscopy (XRFS) using a PANalytical Axios Advanced spectrometer. Fused beads were created by mixing 9g (66% Lithium tetraborate and 34% Lithium metaborate) with 0.9g soil and heating at 1200°C.

2.5 X-ray diffraction (XRD)

2.5.1 Whole-soil preparation

Subsamples of soil from the cores and disaggregated quarry samples were removed and initially ball-milled to a fine powder. In order to achieve a finer and uniform particle-size for powder XRD analysis, a portion of the ball-milled material was micronised under deionised water for 10 minutes with 5 % zincite (National Institute of Standards and Technology (NIST) standard reference material (SRM) 674, ZnO). The addition of an internal standard allows validation of quantification data and also the detection of any amorphous species in the samples. The zincite-spiked whole-soil samples were spray-dried following the method and apparatus described by Hillier (1999). The spray-dried materials were then front-loaded into standard stainless steel sample holders for analysis.

2.5.2 Isolation of a <2 µm fraction

<2µm fractions were isolated using the methodology outlined by Tye et al. (2009).

2.5.3 Oriented mount X-ray diffraction preparation

Approximately 100 mg of the <2 µm material was re-suspended in a minimum of deionised water and pipetted onto a ceramic tile in a vacuum apparatus to produce an oriented mount. The mounts were Ca-saturated using 2 ml 0.1M $CaCl_2.6H_2O$ solution and washed twice to remove excess reagent and allowed to dry at room temperature.

2.5.4 XRD Analysis

XRD analysis was carried out using a PANalytical X'Pert Pro series diffractometer equipped with a cobalt-target tube, X'Celerator detector and operated at 45kV and 40mA. The random powder mounts were scanned from 5-85°2θ at 0.82°2θ/minute. The diffraction data were then initially analysed using PANalytical X'Pert HighScore Plus software coupled to the latest version (2008) of the International Centre for Diffraction Data (ICDD) database. Following identification of the mineral species present in the samples, mineral quantification was achieved using the Rietveld refinement technique (e.g. Snyder & Bish, 1989) using Siroquant v2.5 software. This method avoids the need to produce synthetic mixtures and involves the least squares fitting of measured to calculated XRD profiles. Errors for the quoted mineral concentrations are typically ±2.5% for concentrations >60 wt%, ± 5% for concentrations between 60 and 30 wt%, ±10% for concentrations between 30 and 10 wt%, ±20% for concentrations between 10 and 3 wt% and ±40% for concentrations <3 wt% (Hillier *et al.*, 2001). Where a phase was detected but its concentration was indicated to be below 0.5%, it is assigned a value of <0.5%, since the error associated with quantification at such low levels becomes too large.

2.5.5 Oriented mount analysis

The <2 μm oriented mounts were scanned and analysed using the same approach detailed by Tye *et al*. (2009).

2.6 Scanning Electron Microscope (SEM) analysis

Samples of SR and sandstone were characterised using scanning electron microscopy (SEM) techniques. Samples from the SR borehole were mounted on 10 mm diameter aluminium stubs using conductive carbon cement and examined using Secondary Electron Imaging (SEI). The stub-mounted samples were coated with 250Å of carbon by vacuum evaporation. SEM (SEI) and Back Scatter Election Microscopy (BSEM) observations were undertaken using a LEO 435VP variable pressure SEM instrument, equipped with a solid-state, four-element (diode) backscattered electron detector. The SEM instrument was also fitted with an Oxford INCA energy-dispersive X-ray microanalysis (EDXA) system, which was used to aid mineral identification by interpretation of semi-quantitative micro-chemical information from X-ray spectra recorded simultaneously during SE and BSEM observation. The SEM instrument was operated in conventional high vacuum mode (better than 1 x 10^{-4} torr), with an 10-20 kV electron beam accelerating voltage and beam currents of 100-200 pA for SEI and 300-700 pA for BSEM analysis.

2.7 Calculation of Tau values

Taking the solid phase elemental results we can apply the mass balance model of soil formation developed by Brimhall and co-workers (Brimhall *et al.* 1987; Brimhall *et al.* 1991) and subsequently used by others (e.g. Anderson *et al.* 2001) to examine the extent of elemental losses or gains during soil formation whilst taking into account changes in volume (strain) during pedogenesis. From Amundsen (2003), the mass gains or losses of a given chemical element (j), in the transition from parent material (p) to soil (s) in terms of volume (V), bulk density (ρ) and chemical composition (C) is

$$m_{j,flux} = m_{j,s} - m_{j,p} \qquad \text{eqn. 2}$$

where $m_{j,flux}$ (g cm^{-3}), is the mass (%) of element (j) added/lost (flux) in the soil (s) or the parent material (p). Incorporating volume (cm^3), density (g cm^{-3}), concentration (%) into the model gives

$$m_{jflux} = \frac{V_s \rho_s Cj,_s}{100} - \frac{V_p \rho_p C_j,_p}{100} \qquad \text{eqn. 3}$$

M_{jflux} is the mass of element (j) lost/gained from the parent material volume

$V_s \rho_s C_{j,s}/100$ = mass of element (j) in soil volume of interest and

$V_p\rho_pC_{j,p}/100$ = mass of element (j) in parent material volume

During soil development, volumetric collapse (ΔV) may occur through weathering losses while expansion may occur through biological or physical processes. Volumetric change is defined in terms of strain (ε)

$$\varepsilon i, s = \frac{\Delta V}{Vp} = \left(\frac{Vs}{Vp} - 1\right) = \left(\frac{\rho pCi, p}{\rho sCi, s} - 1\right) \qquad \text{eqn. 4}$$

Where the subscript 'i' refers to the immobile, index element, which in this case is Zr. The fractional mass gain or loss of an element j relative to the mass in the parent material (τ) is defined by combining Equations 2-4:

$$\tau = \frac{mj, flux}{mj, p} = \left(\frac{\rho sCj, s}{\rho pCj, p}(\varepsilon i, s + 1) - 1\right) \qquad \text{eqn. 5}$$

Through substitution, equation 5 reduces to

$$\tau = \frac{Rs}{Rp} - 1 \qquad \text{eqn. 6}$$

Where Rs = $C_{j,s}/C_{i,s}$ and Rp = $C_{j,p}/C_{i,p}$. Thus τ can be calculated readily from commonly available geochemical data and does not require bulk density data.

2.8 Statistical and modelling methods

The objective of the modelling was to use a Monte Carlo simulation based on a simplified version of the Stefan equation (Klene *et al*. 2001) to provide estimates of the depth of 'active layer development' (ALD) during arctic summers. By undertaking this analysis we wished to investigate whether the physical process of freeze thaw was a fundamental control on the depth of the soil-regolith across the outcrop. The outcomes of the Monte Carlo simulation represent a distribution of soil depths across the Sherwood Sandstone outcrop given the assumed statistical distribution for the model parameters and input variables. These could then be compared with the observed frequency of empirical observations made from the boreholes logs.

The ALD modelling was undertaken using the Stefan Equation within a Monte Carlo simulation. Klene *et al*. (2001) suggest that the simplified form of the Stefan solution does not yield an exact solution for thawing, but it does provide an adequate approximation when a single subsurface layer is considered. The form of the Stefan equation used by Klene *et al*. (2001) is

$$z_i = \sqrt{\frac{2k_t s(n_t DDT_a)}{pwL}} \qquad \text{eqn. 7.}$$

Where:

Z_i = Active layer thickness
K_t= Thermal conductivity of the thawed soil (W m^{-1} $°C^{-1}$)
S = Scaling factor of 86400 seconds day^{-1}
N_t = n-factor for the thaw season = (Soil thawing degree days/air thawing degree days)
DDT_a = Air temperature thawing degree day sum (°C days)
P = Bulk density (kg m^{-3})
W = Soil moisture proportion by weight
L = Latent heat of fusion (j kg^{-1})

The Monte Carlo simulation was run in the statistical package ‘R’. We collected proxy data (combined soil surface and air temperature) for current Arctic environments from the Circumpolar Active Layer Monitoring (CALM) website (http://www.udel.edu/Geography/calm/). This allowed us to produce initial estimates of N_t and DDT_a. As climatic conditions for the late Devensian LGM to early Holocene are known to vary considerably we selected data according to the following criteria. During the Loch Lomond stadial (11000 – 10000 yrs BP) in East Yorkshire, England, mean July temperatures of between 9-11°C and winter temperatures as low as -15 to -20°C were found (Walker *et al*. 1993). These temperatures are perhaps slightly warmer than modern day Spitsbergen where Leszkiewicz & Caputa (2004) examined ALD at

Hornsund, Spitsbergen and found the thawed layer extended to ~1.3 m. Thus Spitsbergen was considered a suitable starting point to generate values for the modelling exercise. However, combined soil surface and air temperature data on the CALM website for sites in Spitsbergen were not available. Therefore we selected proxy data from polar sites with latitudes not dissimilar to those of the UK (Table 6). This was essentially a pragmatic exercise to derive a range of realistic values to be used within the Monte-Carlo simulation. We did not attempt to define a specific climate more fully. For values of K_t, P, and W, mean ± 1 standard deviation (SD) values were required. We calculated the SD for each mean value by determining the range of values. This effectively represents the 95% Confidence Interval (CI) which equates to 4 standard deviations. Therefore the range was divided by 4 to give values for SD. More specifically, the following values were used to run the Stefan solution within the Monte Carlo simulation:

K_t - The mean ± SD for the thermal conductivity of thawed soil was given as 1 ± 0.5 on a range extending from 0.15 to 2.24 W m^{-1} $°C^{-1}$. It is envisaged that the soil-regolith-saprolite will be composed of some soil, loose sand and cracked rock. The thermal conductivity of typical solid Sherwood Sandstone Group bedrock is 2.24 W m^{-1} $°C^{-1}$ (Gunn *et al*. 2005) and would represent one end member of the weathered material continuum. The other end of the continuum would be dry sand that has a thermal conductivity of between 0.15 and 0.25 W m^{-1} $°C^{-1}$. Chen (2008) assessed the thermal conductivity of sands with respect to porosity and saturation. Thermal conductivity was found to decrease with increasing porosity whilst increasing moisture contents increased the thermal conductivity for similar porosity values. Where moisture saturation of 0.1 by weight (a typical value for the Sherwood Sandstone Group) was tested, thermal conductivity values of ~1 for sands were reported (Chen, 2008). A further consideration was that at least some of the surface may be moss or lichen covered (the expected dominant vegetation in periglacial environments) at some stage and this will decrease the thermal conductivity compared to that of bare rock (Klene *et al*. 2001).

N_t and DDTa – The mean N_t value calculated from 3 arctic sites (Table 6) was 0.89. Values for DDT_a were calculated from the same data sets as for N_t. The mean value of DDT_a was 940. There is likely to be a strong linear correlation between DDT_a and N_t because the two are related; the sum of the former is used as the denominator in the calculation of the latter. To account for this correlation we simulated a multivariate normal distribution using the MVRNORM function in the MASS library of the R environment (R Development Core Team, 2006). This gave a linear correlation of 0.791 between DDT_a and N_t. We used the function to generate correlated distributions (n=1000) of DDT_a and N_t.

P – Mean bulk density of sandstone bedrock samples (n = 5) from the Bestwood quarry were found to be 2000 kg m^{-3}, whilst top soil bulk density was found to be ~1000 kg m^{-3}. We therefore selected values of 1500 ± 250 kg m^{-3} to be used within the model as it is the average value found across the depth range (Fig 3b).

W – The proportion moisture content by weight value used within the Monte Carlo simulation was 0.1 ± 0.04. These values were based on a compilation of data collected from the archived borehole logs down to depths of 5 m. No knowledge of the yearly precipitation in the Pleistocene exists but an assumption was made that it was similar to the present day. Inevitably during spring melt, saturation of the soils may occur for short periods.

We compared our modeled distribution of 'ALD' depths with (i) the observed borehole data and (ii) a modelled distribution of observations where the data had been declustered. This was undertaken because the sample points are not distributed according to a statistical design and it is evident that they show a degree of clustering (Figure 3). This may affect the raw statistics of the data on soil thickness through oversampling in unrepresentative regions. For instance there are two major clusters along road routes between Northing 360000 and 365000 (Figure 1). When data cannot be treated as independent random variables because they have been obtained by non-random sampling design, a model-based analysis is necessary (de Gruijter *et al.*, 2006). In a model-based analysis we assume that the data are a realization of a spatially correlated random process, and we estimate parameters for the model. This is the fundamental approach in geostatistics. The objective here was to estimate the model mean and variance of SR thickness for the Sherwood Sandstone Group for comparison with expectations under the Stefan Solution. The proposed statistical model is the linear mixed model

$$Z(\mathbf{x}) = \mu + \eta(\mathbf{x}) + \varepsilon(\mathbf{x}), \qquad \text{eqn. 8}$$

where Z is soil depth at location **x**. The model is called a mixed model because it has a fixed effect, μ, which is the mean depth. The other two terms are random effects; η is a spatially auto-correlated second order stationary random variable of mean zero and variance σ^2_1 and ε is an independently and identically distributed random variable of mean zero and variance σ^2_0. The *a priori* variance of the random variable, the variance that is required for comparison to the Monte Carlo output, is $\sigma^2_0 + \sigma^2_1$ and the mean is μ. The estimation of these model parameters was undertaken using residual maximum likelihood (REML). For more detail, the reader is referred to Lark and Cullis (2004). Estimation was undertaken using the LIKFIT procedure in the geoR package for the 'R' statistical platform (Ribeiro and Diggle, 2001)

We undertook exploratory analysis of the data and selected an appropriate transformation (see Results Section 3.1). The linear mixed model was fitted to the transformed data using LIKFIT and the REML option. Models were fitted with exponential, spherical and Matérn covariance functions. The Matérn function failed to converge. Of the other two, the exponential model fitted best, as judged by the maximized residual likelihood (which is a valid basis for selection since the models had common fixed effects and the same number of variance parameters to describe the random effects). The parameters of the exponential model are the two variances, σ^2_0 and σ^2_1, and a distance parameter, *a*, which expresses the autocorrelation of the values of η at two locations $\mathbf{x}_1$ and $\mathbf{x}_2$ by the expression

$$\rho\,(\mathbf{x}_1, \mathbf{x}_2) = \exp\{-|\,\mathbf{x}_1 - \mathbf{x}_2|/a\}. \qquad \text{eqn. 9.}$$

3. Results

3.1 Soil thickness across the outcrop

Figure 2 shows the distribution of soil depths obtained from the borehole logs as previously been reported by Tye *et al*. (2011). Median and mean soil-regolith thickness are ~1.5 and 1.8m respectively. Although occasional values are in excess of 4m, the majority of sites have SR < 2m thick. The potential effects of clustering on the mean and median values of soil thickness were examined using the linear mixed model (Section 2.8) with parameters estimated by residual maximum likelihood (REML). Table 1 shows summary statistics for the original data. These are pronouncedly skew and so were transformed to natural logarithms before further analysis. The transformed data possess a more symmetrical distribution. The REML estimates of the variance parameters and the model mean (transformed soil depth) using the exponential function, are reported in Table 2. The mean and variance of the log-transformed variable, μ_t and σ^2_t, can be transformed back to values on the original scales of measurement, μ_t and σ^2, by the expressions:

$$\mu = \exp\{\mu_t + \sigma^2_t/2\} \quad \text{eqn. 10}$$

$$\sigma^2 = \exp\{2\mu_t + \sigma^2_t\}(\exp\{\sigma^2_t\}-1). \quad \text{eqn. 11}$$

From these we obtain a model mean depth for the soil over the Sherwood Sandstone Group of 2.16 m, and a variance of 2.95 m^2. Note that the mean is somewhat larger than the mean of the raw data, suggesting that there was preferential clustering of observations in areas with shallower soil (Figure 1). The variance of the raw data was somewhat lower than the model *a priori* variance. This is expected when there is clustered sampling since observations within a cluster will tend to be more uniform than a comparable number of independent observations. Figure 4 shows the empirical cumulative frequency distribution of the observed values of thickness and the corresponding model distribution obtained by back-transforming points on the normal frequency distribution with parameters μ_t and σ^2_t.

3.2 Physical Properties of the cores extracted from Sherwood Forest

The penetrometer profile through the soil-regolith shows a marked change in resistance at ~1.7m (Figure 3a), identifying the boundary between the loosely weathered SR and the start of the non-durable rock or saprolite. The depth at which this change in resistance occurs is close to the median and mean depths found in the borehole log survey across the outcrop. Bulk density (B_d) values were calculated (Fig. 3b). In the top 30 cm, a value of 1.03 g cm^{-3} was found, increasing to ~1.5 g cm^{-3} at 30-60 cm depth, with further small progressive increases found with increasing depth. The Porosity (Fig. 3c) was calculated (Eqn. 1) and was ~ 60 % in the top 30 cm, with small decreases with increasing depth to values ~ 40 %. Both the bulk density and porosity results show that below the top 30cm there were relatively small changes within the profile. In particular, there were only small differences found between the base of the regolith and the saprolite or non-durable rock.

3.3 Total Element concentrations in soil-regolith core and bedrock samples

Changes in the total elemental concentrations of the major weathering elements (Ca, Mg, Si, Al, K, Na, Fe and Ti) in each of the 30 cm segments of the core samples extracted from Sherwood Forest (SP3) are shown in Table 3. In addition results of elemental concentrations from the 4 rock samples collected at different depths at Bestwood Quarry and those from the Gamston borehole are reported. The major differences in total elemental concentrations through the soil-regolith-saprolite profile to depths of 3m occur in the top 60cm. There is evidence of CaO enrichment in the top 30 cm, probably through elemental uplift by vegetation and the subsequent recycling of plant material (Jabbágy & Jackobsen, 2004). Both TiO_2 and Zr, considered to be relatively immobile are slightly enriched in the top 30 cm, possibly as a result of the loss of other elements. Within the top 30 cm there were evident decreases in Al_2O_3, SiO_2 and K_2O concentrations compared to the rest of the core; a result of low soil pH (pH ~4 in the top 30 cm) and the dissolution and removal through leaching of minerals such as K-feldspar. Between 30 and 300 cm there was relatively little variation in elemental concentrations. There was a slight increase in concentrations of Al_2O_3 and FeO_3 between 30-60 cm suggesting that the slight increase in soil pH (Table 1) in comparison to the top 30 cm of soil was sufficient for possible re-precipitation of these elements as oxide species.

In the rock samples from the Bestwood Quarry (depths of 3, 6 and 7m), there was generally little variation in elemental concentrations compared to those found in the soil core for most elements. There appeared to be a slight increase in K_2O concentrations, with values rising above 2.5%. Concentrations of CaO and MgO both slightly increase at depths of 7m. However, the bedrock sample collected at 17m has larger concentrations of CaO, K_2O and Na_2O, when compared to the soil samples below 30cm and the shallower rock samples (3, 6 & 7m), suggesting that the weathering process may not have entirely removed the carbonate and gypsum cements at these depths. There is also evidence of larger S concentrations at this depth that may originate from gypsum cements. Elemental analysis of the much deeper (~50m) Gamston borehole sandstone bedrock material shows that concentrations of CaO and MgO are greatly enriched compared to the soil and Bestwood Quarry samples because they still preserve significant amounts of early diagenetic dolomite and calcite cement that have not been leached by weathering experienced at shallower depths (Milodowski *et al*. 1987).

3.4 Calculation of long term weathering losses (Tau)

In this analysis we used the bedrock sample collected from 17m in the Bestwood Quarry. This was selected because it was from a site relatively close to where the soil-regolith-saprolite core was taken. We used measured bulk density values (Fig 3b) and Zr values (Table 1) in the calculation of strain (Fig 3d). A small expansion in the top 30 cm of the soil profile was found, whilst small contractions in the volume of the regolith were found from 30 to 275 cm. Analysis of the percentage of elements lost, incorporating strain are given by values of Tau (equation 6) and are reported (Figures 4a and b). For CaO, values of Tau demonstrate that almost all the Ca that was originally in the soil has been lost suggesting that practically all the carbonate and gypsum cements have been weathered out of the soil and regolith and non-durable rock to depths below 3m. For MgO, K_2O and Na_2O, within the top 30cm, >80 % of the original bedrock concentrations of these elements have been lost. For depths below 30cm, the amount of MgO, Na_2O and K_2O weathered out is < 50 % but values are relatively stable with increasing depth into the non-durable rock. Magnesium (Mg) would be expected to be present in dolomite and ankerite cements but it would also form structural elements in chlorite and smectite clays. For TiO_2,

FeO_3, SiO_2, and Al_2O_3 the greatest losses as determined by Tau were found in the acidic top 30 cm of the profile. Below 30 cm there were much smaller losses and values of Tau were < 0.2 with the exception of SiO_2 which was found to accumulate with depth.

3.5 Mineralogy

Whole rock/soil mineralogical XRD analysis was undertaken on samples from core SP3 and bedrock samples collected from the Bestwood Quarry (Table 4). No evidence of calcite, dolomite or gypsum was found in the soil samples or the Bestwood Quarry samples (6-17m). It is likely that small amounts of these mineral cements may remain, particularly in the deep quarry samples. However, these may have been below the detection limits (~0.5 %) of the XRD instrument. The quarry from which the samples were taken, was in an area previously identified as having the deepest weathering depths to competent bedrock of ~30m across the outcrop (Tye *et al*. 2011). This suggests that greater removal of these cements may have taken place. However, both CaO and S increase in the bedrock sample taken from 17m depth suggesting some gypsum may be present. In the present study, XRD analysis was not undertaken on the Gamston borehole samples. However BSEM-EDXA petrographic analysis of thin sections of sandstone from the Gamston borehole showed that early diagenetic dolomite cement (dolocrete) and later diagenetic ferroan dolomite and ankerite are present (Milodowski *et al*. 1987). Previous work by Bath *et al*. (1987), also identified calcite re-precipitated after dolomite dissolution and $CaCO_3$ concentrations of 2 % were reported. This clearly accounts for the greater CaO, MgO concentrations found in the samples (Table 3).

The XRD data indicate that the core and bedrock samples are predominantly composed of quartz (mean ~83%), with minor amounts of K-feldspar (mean ~13%) and undifferentiated mica species ('mica', possibly including muscovite, biotite and illite) with traces of chlorite, kaolinite, illite/smectite (I/S) and hematite. Overall the major differences were (i) a general increase in K-feldspar concentration with depth, and (ii) a corresponding decrease in quartz concentration with depth. The largest changes within the soil profile can be seen in the acidic top 30 cm. For example, the K-feldspar concentration was 7.9% between 0-30cm, compared to 11-12% between 60 and 300cm. Similarly the concentration of quartz was ~5% higher in the top 30 cm compared to the deeper soil samples. This decrease in K-Feldspar concentration in the top 30 cm can be seen in the decrease in total Al_2O_3 and K_2O concentrations (Table 1). There were no other consistent depth-related patterns found in the concentrations of the other minerals present.

Further XRD analysis of the clay fraction (Table 5) was undertaken to assess whether there was any major alteration of the clay minerals that could aid the disruption of the clay cement of the matrix, thus creating the soil-regolith. The < 2 μm fraction XRD analyses indicate that these are predominantly composed of clay minerals (I/S, illite, kaolinite and chlorite), together with minor-trace amounts of quartz, K-feldspar, albite and possibly cristobalite (Table 5). The composition of the <2 μm fractions indicates that within the 0-300 cm profile, major changes occur only in the most acidic top 30cm. The changes include (i) decreases in chlorite and illite concentrations, probably as a result of alteration to kaolinite with the release of Mg, Fe and K, and (ii) increased kaolinite concentration, partly due to the alteration of chlorite and illite but also through the weathering and alteration of K-feldspar (Table 2). Throughout the rest of the SR core and into the saprolite and bedrock samples there appeared to be no consistent changes in clay mineralogy, and compositional changes may be due to the amount of clay deposited in the sedimentary rock forming process.

3.6 *SEM Analysis*

The degree of cementing by clay particles in various parts of the weathering profile are shown in SEM images (Figure 5). Images of the top part of the profile between 29-33cm (Fig. 5 i & ii) show a relatively open structure; the pore space has developed where the gypsum and carbonate cements have been removed. At depths greater than ~1.7m, the degree of clay cementing appears to be greater, with more clay covering particles (Figures 5iii & iv). These images of a less open structure and the sand particles being held together more tightly, is reflected by the increase in B_d with depth and the decrease in calculated porosity (Figure 3). Figure 5(v) shows again the increase in clay cement holding sand particles together at 220-226cm whilst Figure 5(vi) shows a crescent shape of clay cement after a particle has been removed. These results suggest that the soil-regolith is not only created by the dissolution of the carbonate and gypsum cements but also through the easing apart of the clay cement.

3.7 *Active layer development (ALD) modelling*

The Monte-Carlo simulation based on the Stefan equation was run to obtain a representation of the distribution of likely SR depths across the Sherwood Sandstone outcrop assuming the statistical distribution of the model parameters and input variables. The model output is shown in Figures 6 and 7. Figure 6 shows the relationship between variables and demonstrates the strength of the positive linear (Pearson) correlation (r=0.79) between the simulated values of N_t and DDT_a. Figure 7 shows the empirical cumulative distribution function (CDF) of soil depths generated by the Monte Carlo simulation plotted on the same axes as (i) CDF of raw soil depths obtained from the borehole logs and (ii) the CDF corresponding to the linear mixed model, obtained by generating percentiles of the fitted log-normal distribution. Results show that compared to the raw data and the linear mixed model, the Monte Carlo simulation based on the Stefan equation produced a very similar cumulative distribution of depths with very similar median values. Median values for the raw data and linear mixed model data were 1.5 m and

1.64 m (respectively) and the mean values were 1.8 and 1.76 m, respectively. However, the modelled soil thickness is slightly under-predicted between the 75th and 95th percentiles. The observed borehole SR data included a few values >6m. Originally, these were considered possible Quaternary deposits rather than in-situ weathered material. However, modelled SR thickness also produced some thick soil depths (>6m), suggesting under certain conditions, very deep ALD could occur.

4. Discussion

Tye *et al*. (2011) found a poor relationship between total weathering depth to bedrock and SR depth, suggesting strongly that chemical weathering processes were not the only control on soil-regolith depth. In respect to the chemical weathering process and as a consequence of the Sherwood Sandstone Group being (i) one of the UK's major aquifers and (ii) in the vicinity of proposed high level radioactive waste depositories in the north west of England, the weathering process within the deep rock has been studied in some detail. Burley & Kantorowicz (1986) demonstrated that the porosity of the sandstone is created through the dissolution of the calcite, dolomite and gypsum cements by groundwater. As the Sherwood Sandstone Group is a sedimentary rock unit, there can be variation in the bedrock geochemistry as demonstrated by the bedrock samples collected from Bestwood Quarry or the Gamston Borehole (Table 1). However, if either the Gamston or Bestwood Quarry bedrock samples are used in the calculation of Tau, it is evident that there has been near total removal of the gypsum and carbonate cements. The results show no major differences in the degree of chemical weathering of Ca or Mg within the top 3m of soil-regolith-saprolite weathering continuum. These results support our proposal that regardless of when and how long it took for the chemical removal of the gypsum and carbonate cements, a physical weathering process such as freeze thaw was required to develop the variation in SR thickness across the outcrop.

Our proposed mechanism is that for the SR to develop, the clay cementing and other interlocking grain bonds, needed to be disrupted to produce the loose sand overlying the saprolite. The results from the use of the Stefan equation within the Monte-Carlo simulation suggest strongly that ALD and seasonal freeze thaw is a likely mechanism. In previous research ALD and freeze-thaw processes have been shown to increase the volume of soil, reduce aggregate stability and generally disrupt soil mechanical properties through ice bonding between particles (Wang *et al*., 2007; Kværnø *et al*., 2006). It is also likely that ice will form between cleavage planes of clay minerals, thereby damaging the structure of clays (Konishchev & Rogov, 1993). However, analysis of the physical characteristics of the core suggested that the process of freeze thaw was not overly physically disruptive. The limit of ALD was quite marked in the soil-regolith-saprolite core, notably by the change in penetrometer resistance at ~1.7m. In addition, there was a concomitant increase in bulk density and decrease in porosity through the SR and into the saprolite found with depth, suggesting that the material was becoming more dense and stronger. The rapid change in peneterometer resistance as it goes into the saprolite is because it is entering a material where the sand particles are now being more firmly held together by the clay cement (see Fig 5).

We examined the variables that the Monte Carlo simulation used for each prediction of the thickness of ALD. It was found that the extent of ALD was most sensitive to moisture content with a negative correlation (R^2 = -0.61) (Figure 8). Initially, this appeared to be counter-intuitive when considering the role that water plays in transferring heat through the active layer. However, a soil with greater moisture content will create a greater volume of ice, therefore requiring greater latent energy to change the phase from ice to water in the soil. Thus the thermal conductivity of drier soils, with less ice, may conduct heat downwards more efficiently. Woo and

Xia (1996) examined ground temperature and moisture at two arctic sites; a wetland site and an adjacent pebbly loam site. At both sites, about half of the ground heat flux was consumed by latent heat for ground thawing and that the wetland site had a shallower maximum depth of thaw than the drier site because of the larger ice content in the active layer. Whilst, this modelling exercise represents a simplification of the ALD within the soil system, where a large heterogeneity in the amount of ice present would be expected, the results demonstrate that ALD could be a major control on developing soil thickness across the Sherwood Sandstone Group outcrop. However, there are questions that this study has not been able to address. These include the length of time it has taken to derive the chemical weathering profile and the possible number of cycles of seasonal freeze-thaw and ALD during the Devensian required too produce the distribution of SR thickness observed.

In relation to the previous work published by Tye *et al*. (2011), these results suggest that the non-durable rock or saprolite occurs where the carbonate and gypsum cement has been removed but a physical weathering process to break the clay and grain interlocking bonds has yet to occur. In addition to the dominant role of ALD in developing SR depth, it would be expected that other mechanisms associated with peri-glacial climates have played a role. One mechanism is the frost-cracking of rock before soil development. Anderson (1998) suggested that the rate of the many processes involved with frost cracking depended largely on the length of time spent within a range of sub-zero temperatures designated the ‘frost cracking window’. The creation of new micro-cracks will allow the penetration of water into the rock and initiate the soil development and will be important for subsequent freeze-thaw processes such as ALD. A further mechanism would be the role of plant roots. Tree roots in particular may have played a secondary role in breaking the clay cement and grain interlocking bonds before the vast majority of the Sherwood Sandstone outcrop was deforested in the past 500 years.

5. Conclusions

Results from this study have shown that (i) chemical weathering within the soil-regolith-saprolite has effectively removed the gypsum and carbonate cements, (ii) the soil–regolith depth only differs from the underlying saprolite (or undurable rock) because of the breaking of the clay cement and other grain interlocking bonds and (iii) that periglacial ALD is the major factor in determining the spatial range of soil thicknesses across the outcrop. The role of Quaternary processes on the location and development of soils across the UK has largely focused on the deposition of glacial tills and deposits, the development of sand and gravel river terraces and the formation of soils derived from loess deposits (Catt, 1979). Our hypothesis that the soil-regolith thickness across the Sherwood Sandstone Group outcrop is determined by freeze thaw increases our knowledge of the role of periglacial activity on soil and regolith development in the UK. For example, periglacial activities have been identified as major factors in the development of soils on the chalk downland of southern England. Catt and Hodgson (1976) reported that cryoturbation and freeze thaw processes was responsible for the production of Coombe deposits, the mixing of plateau drift and in the formation of clay-with-flints *sensu-stricto* soils. They reported that the extent of peri-glacial processes and mixing on the clay-with-flints *sensu-stricto* can be as deep as 3m. In this study we have shown that ALD may have helped form SR in excess of 6m on occasion. However, the understanding gained in this study would not have been possible without such extensive legacy borehole datasets and demonstrates their importance in assessing regional scale processes on soil-regolith formation.

Acknowledgements

The authors would like to thank Barry Rawlins for help with the Monte Carlo simulation and Mike Ellis for useful discussion. The paper is published with the permission of the Executive Director of the British Geological Survey.

6. References

Adlam, L.S., Balks, M.R., Seybold, C.A., Campbell, D.I. 2010. Temporal and spatial variation in active layer depth in the McMurdo Sound Region, Antartica. *Antarctic Science*, **22**, 45-52.

Akhurst, M.C., Barnes, R.P., Chadwick, R.A., Millward, D., Norton, M.G., Maddock, R.H., Kimbell, G.S., Milodowski, A.E. 1998. Structural evolution of the Lake District Boundary Fault Zone in west Cumbria, U.K., *Proceedings of the Yorkshire Geological Society,* **52**(2), 139-158.

Allen, D.J., Brewerton, L.J., Coleby, L.M., Gibbs, B.R., Lewis. M.A., MacDonald A.M., Wagstaff, S.J., Williams, A.T. 1997. The physical properties of major aquifers in England and Wales. *British Geological Survey Technical Report WD/97/34 and E.A. R&D 8,* 312pp.

Amundsen, R. 2003. Soil formation, pp.1-35. In *Surface and Ground Water, Weathering and Soils* (ed. J.I. Drever) Vol. 5 *Treatise on Geochemistry* (eds. H.D. Holland and K.K. Turekian), Elsevier-Pergamon, Oxford.

Anderson, R.S. 1998. Near-surface thermal profiles in Alpine bedrock: Implications for the frost weathering of rock. *Arctic and Alpine Research*, **30**, 362-372.

Anderson, S.P., Dietrich, W.E., Brimhall, G.H. Weathering profiles, mass-balance analysis, and rates of solute loss: Linkages between weathering and erosion in a small, steep catchment. *Geological Society of America Bulletin*, **114(9)**, 1143-1158.

Bath, A.H., Milodowski, A.E., Spiro, B. 1987. Diagenesis of carbonate cements in Permo-Triasssic sandstones in the Wessex and the East Yorkshire-Lincolnshire Basins, UK: a stable isotope study. In: Marshall, J.D. (editor). Diagenesis of sedimentary Sequences, Geological Society of London, Special Publication, 36, 173-190.

Berner, R.A., Lasaga, A.C., Garrels, R.M. 1983. The carbonate-silicate geochemical cycle and its effect on atmospheric carbon dioxide over the past 100 million years. *American Journal of Science*, **283**, 641-683.

Braun, J., Heimsath, A.M., Chappell, J. 2001. Sediment transport mechanisms on soil-mantled hillslopes. *Geological Society of America*, **29**, 683-686.

Brimhall, G.H., Dietrich, W.E. 1987. Constitutive mass balance relations between chemical composition, volume, density, porosity and strain in metasomatic hydrochemical systems: Results on weathering and pedogenesis. *Geochimica et Cosmochimica Acta*, **51**, 567-587.

Brimhall, G.H., Lewis, C.J., Ford, C., Bratt, J., Taylor, G., Warin, O. 1991. Quantitative geochemical approach to pedogenesis: importance of parent material reduction, volumetric reduction, and eolian influx in lateritization. Geoderma, 51, 51-91.

Burke, B.C., Heimsath, A.M., White, A.F. 2007. Coupling chemical weathering with soil production across soil-mantled landscapes. *Earth Surface Processes and Landforms*, **32**, 853-873.

Burley, S.D., Kantorowicz, J.D. 1986. Thin section and S.E.M. textural criteria for the recognition of cement-dissolution prosity in sandstones. *Sedimentology*, **33**, 587-604.

Catt, J.A. 1979. Soils and Quaternary geology in Britain. *Journal of Soil Science*, **30**, 607-642.

Catt, J.A., Hodgson, J.M. 1976. Soils and geomorphology of the chalk in south-east England. Earth Surface Processes, 1, 181-193.

Carter, B.J., Ciolkosz, E.J. 1986. Sorting and thickness of waste mantle material on a sandstone spur in central Pennsylvania. *Catena*, **13**, 241-256

Carter, B.J., Ciolkosz, E.J. 1991. Slope gradient and aspect effects on soils developed from sandstone in Pennsylvania. *Geoderma,* **49**, 199-213.

Chen, S.X. 2008. Thermal conductivity of sands. *Heat Mass Transfer*, **44,** 1241-1246.

Davies, W.M. 1892. The convex profile of badland divides. *Science*, **20**, 245.

De Gruijter, J., Brus, D., Bierkens, M., Knotters, M. 2006. *Sampling for natural resource monitoring.* Springer, Berlin.

Edwards, W.N. 1967. Geology of the country around Ollerton. Memoirs of the Geological Survey of Great Britain, HMSO, pp.297.

Fernandes, N.F., Dietrich, W.E. 1997. Hillslope evolution by diffusive processes: The timescale for equilibrium adjustments. *Water Resources Research*, **33**, 1307-1318.

Gilbert, G.K. 1909. The convexity of hilltops. *Journal of Geology*, **17**, 344-350.

Gunn, D.A., Jones, L.D., Raines, M.G., Entwisle, D.C., Hobbs, P.R.N. 2005. Laboratory measurement and correction of thermal properties for application to rock mass. *Geotechnical and Geological Engineering*, **23**, 773-791.

Heimsath, A.M., Dietrich, W.E., Nishiizumi, K., Finkel, R.C. 1997. The soil production function and landscape equilibrium. *Nature*, **388**, 358-361.

Heimsath, A.M., Dietrich, W.E., Nishiizumi, K., Finkel, R.C. 2001. Stochastic processes of soil production and transport: Erosion rates, topographic variation and cosmogenic nuclides in the Oregon Coast Range. *Earth Surface Processes and Landforms,* **26**, 531-552.

Heimsath, A.M., Fink, D., Hancock, G.R. 2009. The ‘humped’ soil production function: eroding Arnhem Land, Australia. *Earth Surface Processes and Landforms*, **34**, 1674-1684.

Hillier, S. 1999. Use of an air-brush to spray dry samples for X-ray powder diffraction. *Clay Minerals*, **34**, 127-135.

Hillier, S., Suzuki, K., Cotter-Howells, J. 2001. Quantitative determination of Cerussite (lead carbonate) by X-ray powder diffraction and inferences for lead speciation and transport in stream sediments from a former lead mining area of Scotland. *Applied Geochemistry*, **16**, 597-608.

Howard, A.S.; Warrington, G.; Carney, J.N.; Ambrose, K.; Young, S.R.; Pharaoh, T.C.; Cheney, C.S.; Ball, D.F.; Brandon, A.; Charsley, T.J.; Crofts, R.G.; Dean, M.T.; Giles, J.R.A.; Glover, B.W.; Lawley, R.S.; Lowe, D.J.; Rathbone, P.A.; Waters, C.N.; Ivimey-Cook, H.C.; Riley, N.J.; Bloodworth, A.J.; Forster, A.; Royles, C.P. 2009. Geology of the country around Nottingham. Memoir for 1:50000 geological sheet 126. HMSO, London. pp.151-170.

Hren, M.T., Hilley, G.E., Chamberlain, C.P. 2007. The relationship between tectonic uplift and chemical weathering rates in the Washington Cascades: Field measurements and model predictions. *American Journal of Science*, **307**, 1041-1063.

Jobbágy, E.G., Jackson, R.B., 2004. The uplift of soil nutrients by plants: biogeochemical consequences across scales. *Ecology*, **85 (9)**, 2380–2389.

Klene, A.E., Nelson, F.E., Shiklomanov, N.I. 2001. The N-factor as a tool in geocryological mapping: Seasonal thaw in the Kuparuk river basin, Alaska. *Physical Geography*, **22**, 449-466.

Konishev, V.N., Rogov, V.V. 1993. Investigations of cryogenic weathering in Europe and Northern Asia. *Permafrost and Periglacial Processes*, **4**, 49-64.

Kvænø, S.H., Øygarden, L. 2006. The influence of freeze-thaw cycles and soil moisture on aggregate stability of three soils in Norway. *Catena,* **67,** 175-182.

Langton, D.D 1999. The Panda lightweight penetrometer for soil investigation and monitoring material compaction. *Ground Engineering*, **September 1999**, 33-37.

Lark, R.M., Cullis, B.C. 2004. Model-based analysis using REML for inference from systematically sampled data on soil. *European Journal of Soil Science* **55**, 799–813.

Leszkiewicz, J., Caputa, Z. 2004. The thermal condition of the active layer in the permafrost at Hornsund, Spitsbergen. *Polish Polar Research*, **25**, 223-239.

McKean, J.A., Dietrich, W.E., Finkel, R.C., Southon, J.R., Caffee, M.W. 1993. Qunatification of soil production and downslope creep rates from cosmogenic ^{10}Be accumulations on a hillslope profile. Geology, 21, 343-346.

Milodowski, A.E., Strong, G.E., Wilson, K.S., Holloway, S., Bath, A.E. 1987. Diagentic influences on the aquifer properties of the Permo-Triassic sandstones in the East Yorkshire and Lincolnshire Basin. British Geological Survey Internal Report WJ/GE/87/002.

Milodowski, A.E., Gillespie, M.R., Naden, J., Fortey, N.J., Shepherd, T.J., Pearce, J.M., Metcalfe, R. 1998. The petrology and paragenesis of fracture mineralization in the Sellafield area, west Cumbria. *Proceedings of the Yorkshire Geological Society*, **52**(2), 215-241.

Minasny, B., McBratney, A.B. 1999. A rudimentary mechanistic model for soil production and landscape development. *Geoderma*, **90**, 3-21.

Molnar, P., Anderson, R.S., Prestrud Anderson, S. 2007. Techtonics, fracturing of rock, and erosion. *Journal of Geophysical Research*, **112**, F03014.

Mudd, S.M., Furbish, D.J. 2004. Influence of chemical denudation on hillslope morphology. *Journal of Geophysical Research*, **109**, F02001.

Phillips, J.D., Marion, D.A., Lucklow, K., Adams, K.R. 2005. Nonequilibrium regolith thickness in the Ouachita Mountains. *The Journal of Geology*, **113,** 325-340.

Phillips, J.D. 2010. The convenient fiction of steady-state soil thickness. *Geoderma*, **156**, 389-398.

R Development Core Team 2006. R: A language and environment for statistical computing. R Foundation for Statistical Computing, Vienna.

Ragg, J.M., Beard, G.R., George, H., Heaven, F.W., Hollis, J.M. Jones, R.J.A., Palmer, R.C., Reeve, M.J., Robson, J.D., Whitfield, W.A.D. 1984. *Soils and their use in Midland and Western England. Soil Survey of England and Wales Bulletin No. 12.* MAFF, Harpenden, pp. 433.

Ribeiro, P.J., Diggle, P.J. 2001. geoR: a package for geostatisticsal analysis. *R-NEWS*, **1**, 15–18.

Riggins, S.G., Anderson, R.S., Anderson, S.P., Tye, A.M. 2011. Solving a conundrum of a steady-state hilltop with variable soil depths and production rates, Bodmin Moor, U.K. *Geomorphology*, **128**, 73-84.

Roering, J.J., Kirchner, J.W., Sklar, L.S., Dietrich, W.E. 2001. Hillslope evolution by nonlinear creep and landsliding: An experimental study. *Geology*, **29**, 143-146.

Small, E.E., Anderson, R.S., Finkel, R. (1999) Erosion rates of summit flats using cosmogenic radionuclides. *Earth and Planetary Science Letters,* **150,** 413-425

Smith, E.G., Rhys, G.H., Goossens, R.F. 1973. Geology of the Country around East Retford, Worksop and Gainsborough. Memoirs of the Geological Survey of Great Britain, HMSO, pp.348.

Smith, P.D., Thomasson, A.J. 1982. Density and water-release Characteristics. In Soil Survey Laboratory Methods. Soil Survey Technical Monograph No. 6. Eds. B.W. Avery and C.L. Bascomb, Harpenden.

Snyder, R.L., Bish, D.L. 1989 *Quantitative analysis*, in Modern powder diffraction, Bish, D.L., e Post, J.E. (eds) Reviews in mineralogy vol. 20, Mineralogical Society of America, 101-144.

Spink, T.W., Norbury, D.R. 1993. The engineering geological description of weak rocks and overconsolidated soils, In *The Engineering Geology of Weak Rock.* Coulthard, J.M. & Cripps, J.C. (eds.), Balkema, Rotterdam, pp.289-301.

Tye, A.M., Kemp, S.J., Poulton, P.R. 2009. Responses to soil clay mineralogy in the Rothamsted Classical Experiments in relation to management practice and changing land use. *Geoderma*, 153, 136-146.

Tye, A.M., Lawley, R.L., Ellis, M.A., Rawlins, B.G. 2011. The spatial variation of weathering and soil depth across a Triassic sandstone outcrop. *Earth Surface Processes and Landforms*, **36**, 569-581.

Walker, M.J.C., Coope, G.R., Lowe, J.J. 1993. The Devensian (Weichselian) late-glacial paleoenvironmental record from Gransmoor, East Yorkshire, England. *Quaternary Science Reviews,* **12(8),** 659-680.

Wang, D-Y., Ma, W., Niu, Y-H, Chang, X-X., Wen, Z. 2007. Effects of cyclic freezing and thawing on mechanical properties of Qinghai-Tibet clay. *Cold Regions Science and Technology*, **48**, 34-43.

Wollschalager, U., Gerhards, H., Yu, Q., Roth K. 2010. Multi-channel ground penetrating radar to explore spatial variations in thaw depth and moisture content in the active layer of a permafrost site. *The Cryosphere,* **4**, 269-283.

Woo, M.k., Xia, Z. 1996. Effects of hydrology on the thermal conditions of the active layer. *Nordic Hydrology*, **27**, 129-142.

Yoo, K., Amunson, R., Heimsath, A.M., Dietrich, W.E. 2005. Process based model linking pocket gopher (Thomomys bottae) activity to sediment transport and soil thickness. *Geological Society of America*, **33**, 917-920.

Yoo, K., Mudd. S.M., Sanderman, J., Amundseon, R., Blum, A. 2009. Spatial patterns and controls of soil chemical weathering rates along a transient hillslope. *Earth and Planetary Science Letters*, **288**, 184-193.

Table 1: Summary statistics of soil-regolith thickness data prior and after log transformation.

	Original data (m)	**Log Transformed data (Log_e m)**
Average	1.88	0.63
Median	1.5	0.41
SD	1.41	0.68
Skew	2.26	-0.14
Octile skew	0.26	-0.13
Min	0.15	-1.9
Max	9.1	2.21
Q1	1	0
Q2	2.44	0.89
N	256	256

Table 2: REML estimates of the variance parameters and the model mean transformed soil depth for the linear mixed model (eqn. 2) for log-transformed soil thickness

Variance Parameter	**Value**
σ^2_0	0.256
σ^2_1	0.236
a	1714m
Mean (ln m)	0.5225

Table 3: Total concentrations of major elements in Sherwood Sandstone Soil-regolith-saprolite profile and bedrock samples from Bestwood Quarry and the Gamston Borehole.

Sample	Depth (m)	CaO %	MgO %	SiO_2 %	Al_2O_3 %	K_2O %	Na_2O %	FeO_3 %	TiO_2 %	Zr mg kg^{-1}	S mg kg^{-1}	Cl mg kg^{-1}
SP 3(1)	0.15	0.08	0.07	86.3	2.99	1.31	0.12	0.99	0.21	214.9	476	106
SP 3(2)	0.45	0.04	0.24	87.2	5.83	2.43	0.14	1.35	0.17	107.5	296	42
SP 3(3)	0.75	0.04	0.20	89.8	5.01	2.50	0.14	0.85	0.13	83.1	238	26
SP 3(4)	1.05	0.04	0.20	90.1	4.68	2.32	0.13	0.99	0.12	90.1	293	35
SP 3(5)	1.35	0.03	0.19	89.7	4.84	2.48	0.13	0.91	0.12	83.1	264	34
SP 3(6)	1.65	0.04	0.20	89.3	4.84	2.46	0.13	0.96	0.13	80.1	250	47
SP 3(7)	1.95	0.05	0.19	90.8	4.51	2.29	0.12	0.83	0.12	77.0	204	32
SP 3(8)	2.25	0.04	0.18	90.4	4.46	2.26	0.13	0.98	0.12	78.8	232	46
SP 3(9)	2.55	0.04	0.17	91.3	4.15	2.14	0.12	0.78	0.10	66.9	236	59
BW 4a	3	0.01	0.17	89.2	5.25	2.70	0.14	0.89	0.11	74.8	173	44
BW 1f	6	0.02	0.18	89.6	5.09	2.75	0.15	0.61	0.11	71.3	267	52
BW 1e	7	0.06	0.28	86.4	6.29	2.86	0.14	2.12	0.35	387.4	101	58
BW 2a	17	0.42	0.30	86.5	6.16	3.03	0.21	1.30	0.16	86.5	484	1312
Gam 1	50	1.38	1.6	89.3	6.3	2.44	0.10	1.5	0.18	106	324	53
Gam 2	50	3.88	4.1	80.7	4.6	1.84	0.10	1.17	0.13	85	416	129
Gam 3	50	1.65	1.8	87.9	4.8	1.86	0.10	1.47	0.16	102	374	80

SP = Sherwood Pines Soil-regolith-saprolite core

BW = Bestwood Quarry Rock samples

Gam = Gamston Borehole, Lincolnshire.

Table 4: Whole rock (< 2 mm) XRD analysis (%) of Sherwood sandstone soil-regolith profile (SP3) and quarry samples collected from Bestwood Quarry.

	Depth (m)	Quartz	K-feldspar	'mica'	Kaolinite	Chlorite	Illite/smectite	hematite
SP 3(1)	0.15	88.6	7.9	2.2	0.8	BD	<0.5	<0.5
SP 3(2)	0.45	82.3	12.1	2.6	1.2	0.7	0.7	<0.5
SP 3(4)	1.05	84.0	11.7	1.8	1.2	0.5	0.5	<0.5
SP 3(7)	1.95	83.0	12.4	2.2	1.1	0.5	0.5	<0.5
SP 3(8)	2.25	84.2	11.5	1.8	1.2	0.5	0.5	<0.5
BW 4a	3	84.0	15.6	<0.5	<0.5	<0.5	<0.5	<0.5
BW 1f	6	82.2	14.9	2	0.7	<0.5	<0.5	<0.5
BW 1e	7	76.8	15.8	3.7	2.6	<0.5	<0.5	0.8
BW 2a	17	78.9	16.8	2.5	1.3	<0.5	<0.5	<0.5

Table 5: < 2 μm clay and non-clay mineralogy from the borehole SP3 taken in Sherwood Forest and bedrock samples taken from Bestwood Quarry.

Sample	Depth (m)	% clay mineral			Non-clay minerals
		I/S	Illite	Kaolinite	
SP 3(1)	0.15	34	19	45	quartz, K-feldspar, albite
SP 3(2)	0.45	18	37	31	quartz, K-feldspar, albite
SP 3(4)	1.05	37	30	23	quartz, K-feldspar, albite
SP 3(7)	1.95	38	35	20	quartz, K-feldspar, albite
SP 3(8)	2.25	36	28	26	quartz, K-feldspar
BW 4a	3	34	42	15	quartz, albite, K-feldspar, ?cristobalite
BW 1f	6	53	19	26	quartz
BW 1e	7	81	7	10	quartz
BW 2a	17	54	20	25	quartz, hematite

Table 6: Review of parameters obtained from datasets obtained from the CALM website for use in the Stefan solution (Eqn. 4) to predict the potential distribution of 'active layer development' depths across the Sherwood Sandstone outcrop in Nottinghamshire.

Site	Year	Latitude / Longitude	Soil Thawing degrees days *	Air Thawing degree days *	n-factor (Nt)**
Marre Sale, West Siberia	2007	69°N 66°E	846	803	1.05
Parsons Lake, Canada	1990	65°N 133°W	831	1068	0.77
Cape Rogozhny, NE Siberia	1996	65°N 176°E	818	947	0.86

* Sum of temperatures above freezing when soil temp > 0
** Dimensionless

Figure Headings:

Figure 1: Distribution of borehole logs across the study area. Data for borehole depths is separated into quartiles. The graph shows clustering of the archive borehole data in some areas where many boreholes have been taken for specific engineering projects. Coordinates are metres on the British National Grid.

Figure 2: The empirical cumulative distribution function of soil-regolith thickness across the Sherwood Sandstone obtained from the archive borehole logs (n=282) (+) and the corresponding distribution function from the linear mixed model (Eqn. 2).

Figure 3: Graphs showing changes in physical characteristics through the Sherwood sandstone profile with depth; (a) penetrometer resistance, (b) bulk density (g cm^{-3}), (c) porosity (%) and (d) strain.

Figure 4: Values of Tau (τ) for elements showing the proportion of elements depleted or enriched by the weathering process. A Tau value of zero indicates no gain or loss.

Figure 5: SEM photos showing the extent of clay cementing through the profile of the Sherwood Sandstone soil-regolith. Figures (i) & (ii) are taken from 29-33cm depth. They show a relatively open sand grain structure although some clay forming a grain coating meniscus is observed to weakly bind or cement sand grains. Figure (iii) shows the more clay-rich sandstone matrix at 108-112cm. There appears a less open structure than at the top of the profile. Figure (iv) shows how the binding of particles by clay occurs at 222-226cm. Figure (v) shows the structure at 260-264cm where the clay binding is more evident. Figure (vi) shows a residual meniscus of clay particles left after a sand grain has been removed.

Figure 6: Relationship between values of four variables used in the Monte-Carlo simulation (n=1000) of the Stefan equation

Figure 7: The empirical cumulative distribution function of soil-regolith thickness across the Sherwood Sandstone obtained from the archive borehole logs (n=282) (+), the corresponding distribution function for the linear mixed model (solid line) and the values of thickness generated by the Monte Carlo simulation (•).

Figure 8: Scatterplot showing the relationship between 'Active Layer Thickness' estimated by the Stefan equation and the moisture content (proportion by weight) values used within the Monte Carlo simulation.

Fig 1:

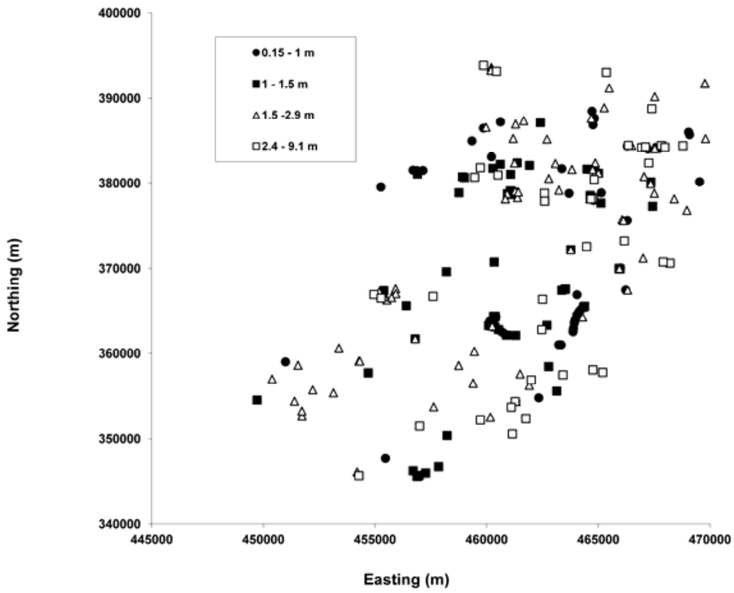
400000
390000
380000
370000
360000
350000
340000
Northing (m)
445000
450000
455000
460000
465000
470000
Easting (m)
0.15 - 1 m
1 - 1.5 m
1.5 -2.9 m
2.4 - 9.1 m

Fig 2:

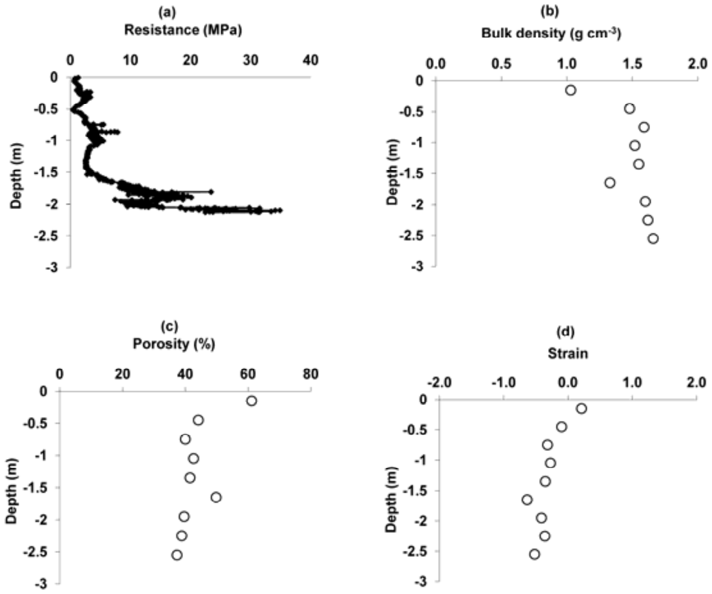
(a)
Resistance (MPa)
0
10
20
30
40
Depth (m)
0
-0.5
-1
-1.5
-2
-2.5
-3
(b)
Bulk density (g cm-3)
0.0
0.5
1.0
1.5
2.0
(c)
Porosity (%)
0
20
40
60
80
(d)
Strain
-2.0
-1.0
0.0
1.0
2.0

Fig 3:

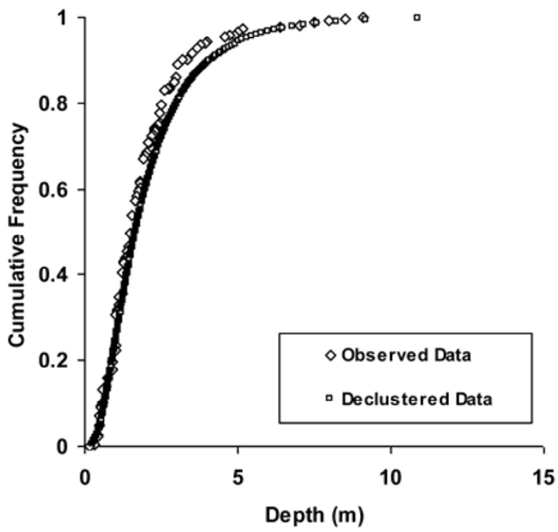

Cumulative Frequency
1
0.8
0.6
0.4
0.2
0
Observed Data
Declustered Data
0
5
10
15
Depth (m)

Fig 4:

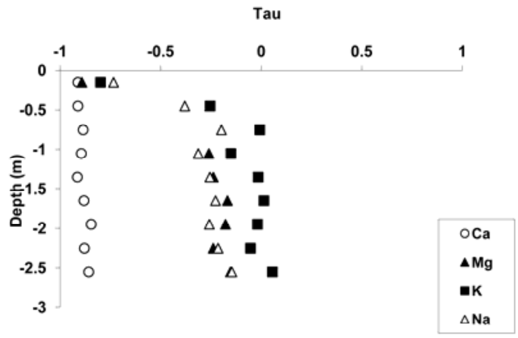
Tau
-1
-0.5
0
0.5
1
0
-0.5
-1
-1.5
-2
-2.5
-3
Depth (m)
Ca
Mg
K
Na

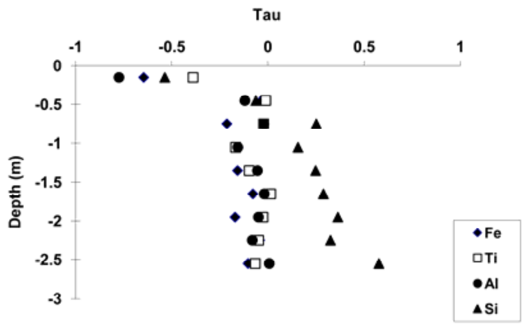
Tau
-1
-0.5
0
0.5
1
0
-0.5
-1
-1.5
-2
-2.5
-3
Depth (m)
Fe
Ti
Al
Si

Fig 5:

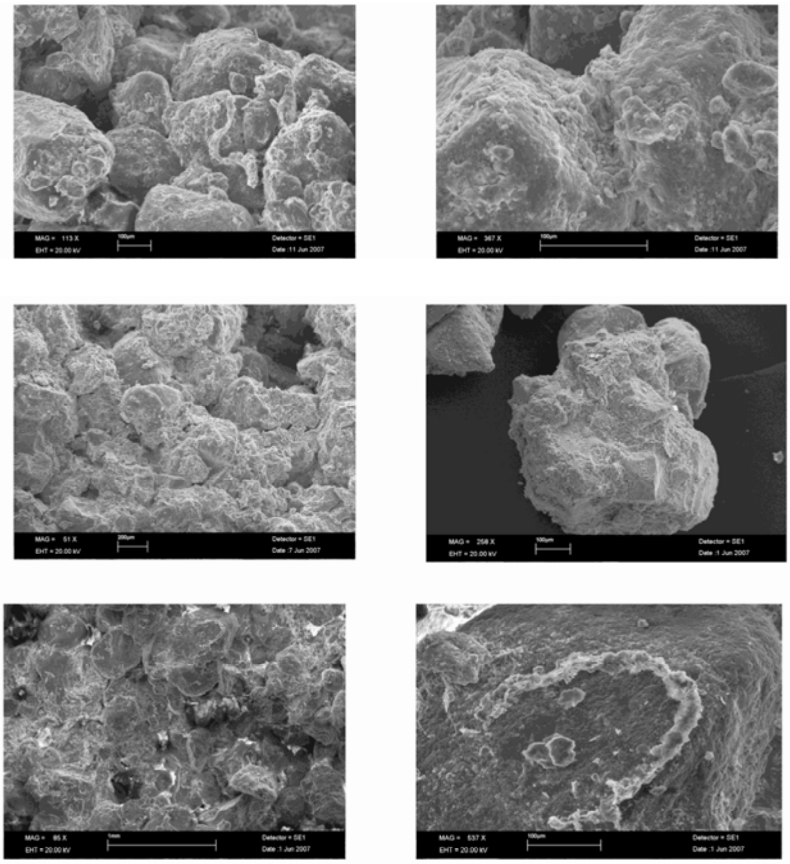
MAG = 113 X
EHT = 20.00 kV
100µm
Detector = SE1
Date :11 Jun 2007
MAG = 367 X
EHT = 20.00 kV
100µm
Detector = SE1
Date :11 Jun 2007
MAG = 51 X
EHT = 20.00 kV
200µm
Detector = SE1
Date :7 Jun 2007
MAG = 258 X
EHT = 20.00 kV
100µm
Detector = SE1
Date :1 Jun 2007
MAG = 85 X
EHT = 20.00 kV
1mm
Detector = SE1
Date :1 Jun 2007
MAG = 537 X
EHT = 20.00 kV
100µm
Detector = SE1
Date :1 Jun 2007

Fig 6:

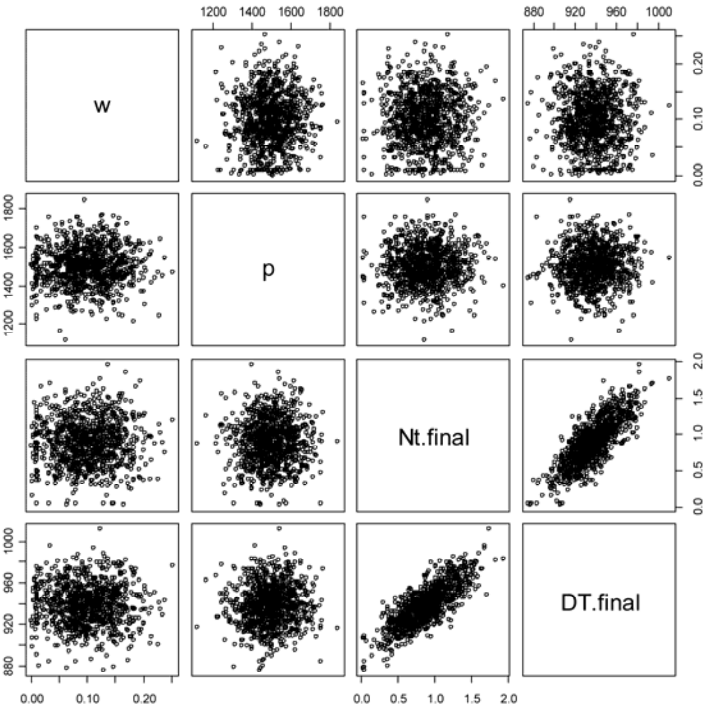

w
p
Nt.final
DT.final
1200 1400 1600 1800
880 920 960 1000
0.00 0.10 0.20
0.0 0.5 1.0 1.5 2.0

Fig 7:

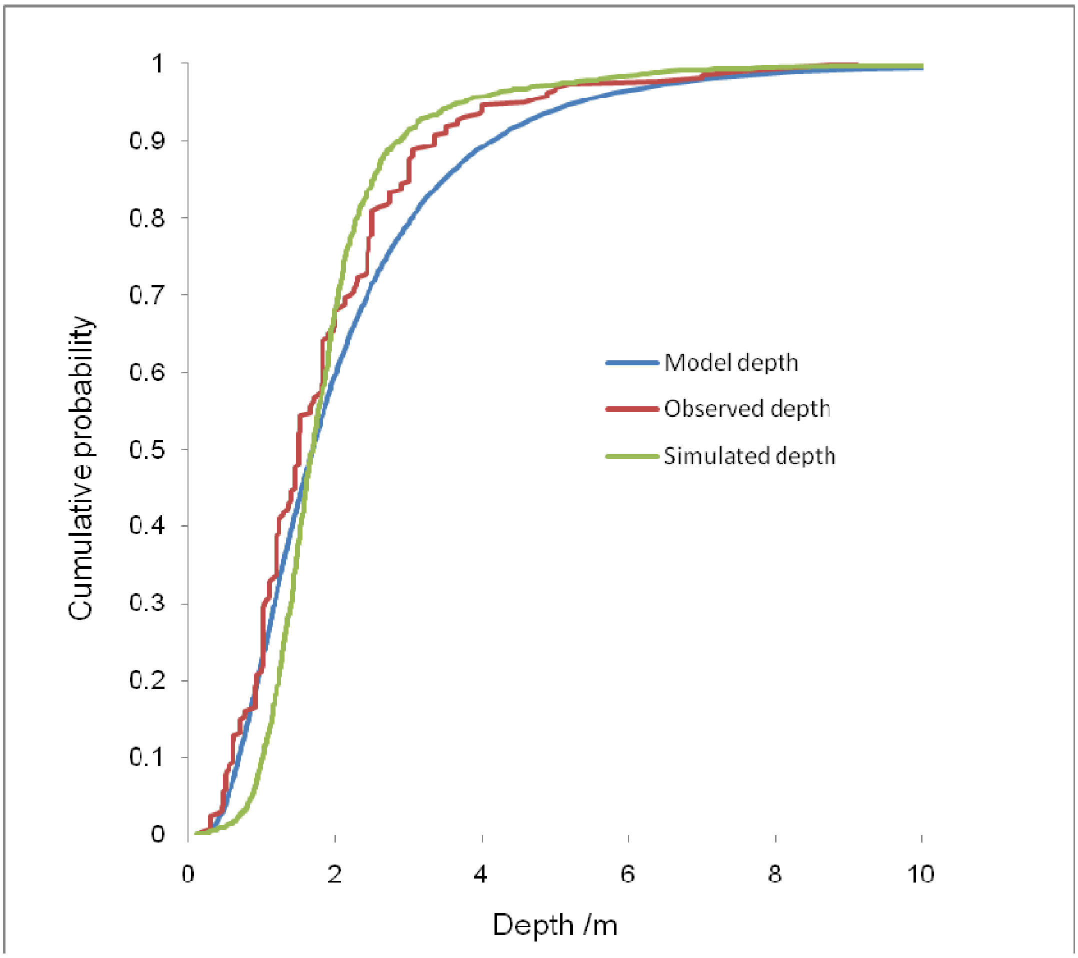

Cumulative probability
1
0.9
0.8
0.7
0.6
0.5
0.4
0.3
0.2
0.1
0
0
2
4
6
8
10
Depth /m
Model depth
Observed depth
Simulated depth

Fig 8:

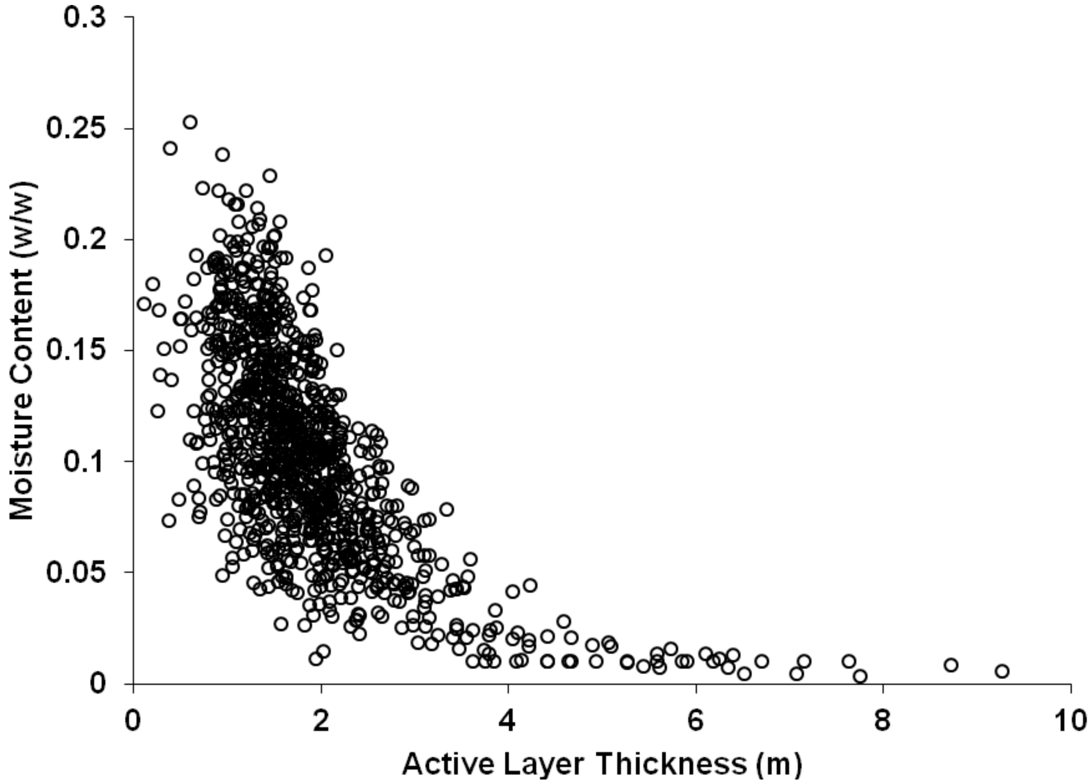
0.3
0.25
0.2
0.15
0.1
0.05
0
Moisture Content (w/w)
0
2
4
6
8
10
Active Layer Thickness (m)